THERMOPHYSICAL CHARACTERISTICS AND EVOLUTION OF REGOLITH ON LUNAR IMPACT MELTS. C. L. Gallinger[1] and R. R. Ghent[1,2], [1]Dept of Earth Sciences, University of Toronto (Toronto, ON, Canada, cailin.gallinger@mail.utoronto.ca), [2]Planetary Science Institute, Tucson, AZ.

Introduction: The rate of development and overturning of regolith throughout the Moon's history is an important constraint in understanding the age of lunar surfaces and their associated features. To date, the Moon remains the only planetary body for which radiometric ages tied to specific impact events and geologic features exist. Correlating the size-frequency distribution of superimposed impact craters (CSFD) on these surfaces to absolute ages of associated samples has been the basis for estimating the age of other regions for which we do not have direct samples, both on the Moon and elsewhere in the solar system. These ages also provide constraints for estimating the rates of overturn of regolith on the lunar surface, and by extension the depth of resurfacing for a particular age [1]. However, the link between the physical processes that produce and overturn regolith and the time scales over which they operate is still not well constrained. Because large impact melt ponds and flows are relatively uniform and solid when they are emplaced, they represent a valuable opportunity to investigate the process of regolith formation on "fresh" rock surfaces. In this work, we present analysis of the thermophysical characteristics of impact melt associated with young lunar craters. These properties are controlled by the physical properties—largely, density—of the materials from the surface to ~1 meter depth. We examine both ponds and flows of various ages.

Previous studies have described the identification of impact melt on the Moon using radar [e.g., 2-4] and image data [e.g., 5-9]. The thermal properties of some large impact melts have been documented [10-14], but the relationship between the thermophysical properties of impact melt and age has not yet been investigated. Here, we investigate impact melt associated with 26 craters identified as containing melt external to their rims [3] for their thermal properties as revealed by the Diviner instrument onboard the Lunar Reconnaissance Orbiter spacecraft.

Mapping: Using the list of [3], we mapped melt flows and/or ponds for the 26 craters for which these deposits were prominent and easily identified. We preferentially selected melt ponds where possible, as their surfaces are likely to have experienced the least mass-wasting or other modification processes over their lifetimes, which would contaminate the signal of aging and regolith development. When melts were difficult to identify, we used multiple datasets (LROC NAC images, LOLA altimetry/slope data, Mini-RF radar backscatter, Diviner average nighttime temperature) to find areas with geomorphological and remote-sensing properties distinct from the rest of the crater ejecta blanket.

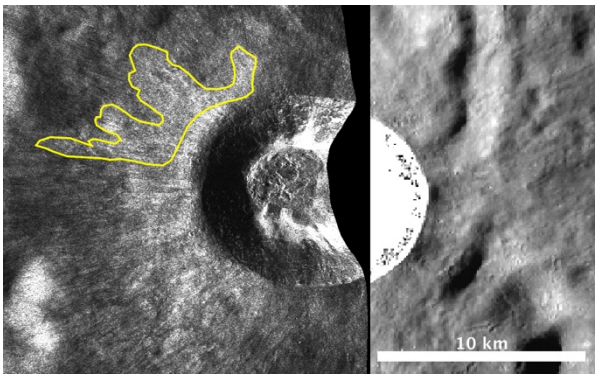

Fig. 1: Impact melt mapped at Furnerius A, an 11 km diameter crater. Mini-RF total backscattered power over LROC WAC mosaic. Impact melt appears as a high-backscatter lobate layer on one side of the crater. Yellow line indicates location of Diviner data used here.

Data and Methods: We analyzed the nighttime temperatures of the melt regions, which are controlled by thermophysical properties, using data from the Diviner Lunar Radiometer Experiment [15]. For this study, we used data from channels 6-8 (12.5-100 μm) to extract regolith temperature and rock abundance, following the algorithm of [10]. We used data from the beginning of the LRO mapping cycle orbits (September 9, 2009) to November 1, 2019. In this time LRO, has completed over 45,000 orbits, and Diviner has gone through 127 complete mapping cycles of the lunar surface, resulting in greatly increased local time coverage compared to previous analyses, especially for small, localized regions.

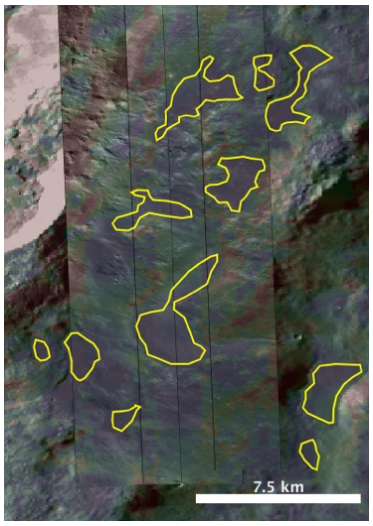

Fig. 2: Example of impact melt mapping at Tycho crater (85 km diameter), where large melt pools are found on the south-eastern and north-eastern rims. Base map is LROC NAC stamps overlain on LROC WAC mosaic. As a check against morphology, the LOLA 1024 ppd slope map was also used to ensure mapped regions came from flat surfaces (< 5° slope).

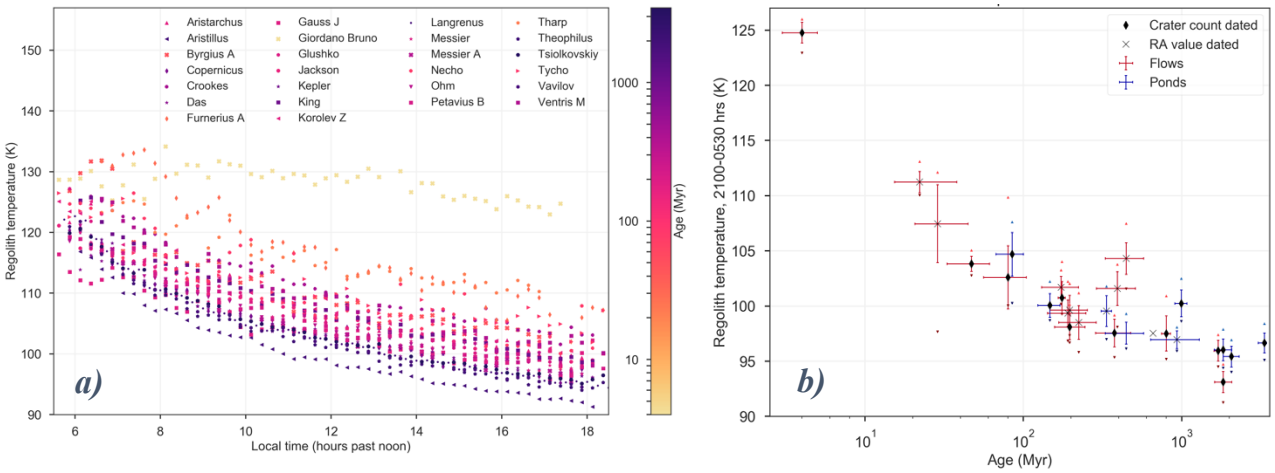

Fig. 3 a) 0.25 hr-binned nighttime regolith temperatures for 26 craters with published ages, corrected to equivalent equatorial values. b) Average nighttime temperatures from 2100-0530 hrs lunar local time, plotted against age. Vertical error bars are ±1σ. Small triangles indicate maximum and minimum temperatures for each crater. In both plots, ages are estimated either from superimposed ejecta blanket CSFD or the rock abundance relation of [17].

Data Processing. We used the algorithm of [10] to extract regolith temperature from Diviner data that we projected and binned to 128 ppd using the 2D Monte Carlo algorithm of [11], and corrected for local topography [14]. For comparisons, data were normalized to equivalent equatorial temperatures.

Results: We observe a distinct decrease in derived nighttime regolith temperatures with increasing age (Fig. 3 a). Additionally, the slopes of these temperatures through the lunar night increase with age, especially in the first ~100 Myr. A plot of crater age vs average regolith temperature for the post-twilight to pre-dawn period (Fig. 3b) shows a gradual flattening with age, perhaps reflecting the increasing dominance of regolith overturning rather than regolith thickening with age [1].

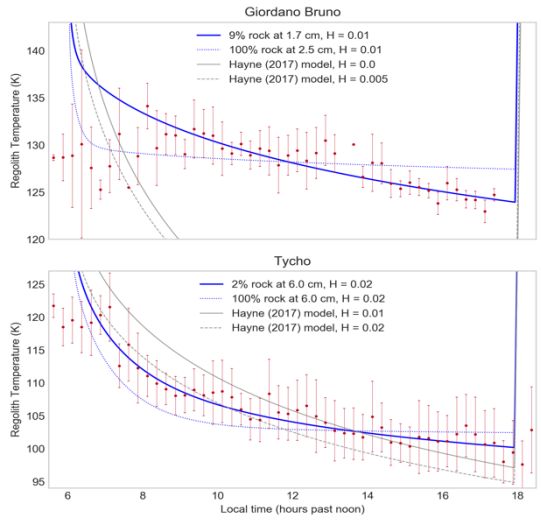

Fig. 4: Plot of nighttime temperature data for craters Giordano Bruno (a.m.a.= 4±1.2 Myr) and Tycho (a.m.a.= 85^{+15}_{-18} Myr)[17], with four thermophysical models overlain. In grey are two models based on that of [14] with no buried rock layer. In blue are two thermal models showing a buried fractional rock (solid) and solid rock (dotted) layer.

Modelling: We modified the 1D thermal model from [16] to include the variable thermal properties of [14] and linear mixing of rock and regolith properties to examine the potential thermophysical structure giving rise to the observed temperature curves. We predicted that a modelled semi-infinite solid rock layer overlying a layer of regolith would reproduce the observed signature of regolith developing from breakdown of a solid melt flow. However, in order to match the observed temperature curves, we had to use rock fractions of only 2-9% (Fig. 4). No pure-regolith model could match the observed data. This suggests there may be a more complicated process generating regolith on impact melts, perhaps including a transitional layer of rock-regolith mixing and additional blankets of regolith deposited from distal impacts over time.

References: [1] Costello et al. 2018, *Icarus*, 314, 327–344, doi:10.1016/j.icarus.2018.05.023. [2] Carter et al. 2012, *JGR Planets*, 117(2):1-13. [3] Neish et al. 2014, *Icarus*, 239:105-117. [4] Neish et al. 2017, *Icarus*, 281:73-89. [5] Strom & Fielder, 1970, *Comm. Lun. Planet. Lab.*, 8:235-288. [6] Shoemaker et al. 1968, *JGR* 73(12):3989-4043. [7] Hawke & Head 1977, *Impact and Explosion Cratering*, 815-841. [8] Cintala & Grieve, 1998, *Meteor. Planet. Sci*, 33(4):889-912. [9] Plescia & Cintala 2012, *JGR Planets* 117(3):1-12. [10] Bandfield et al. 2011, *JGR Planets* 116(E12):1-18. [11] Williams et al. 2016, *Icarus*, 273: 205-213. [12] Ghent et al. 2016, *Icarus* 273 (2016) 182–195. [13] Greenhagen et al. 2016, *Icarus*, 273:237-247. [14] Hayne et al. (2017), *JGR Planets*122(12): 2371-2400. [15] Paige et al. (2010), *Space Sci Rev*, 150(1-4):125-160. [16] https://github.com/nschorgh/Planetary-Code-Collection [17] Ghent et al. 2014, *Geology*, 42 (12); 1059–1062, doi:10.1130/G35926.1.